Relative Formation Rate Constants and Electronic-State Distributions of Ne* Produced from the Ne^+/SF_<6^-> and Ne^+/C_6F_<6-> Ion-Ion Neutralization Reactions in the He Flowing Afterglow

TSUJI, Masaharu
Institute for Materials Chemistry and Engineering, and Research and Education Center of Green Technology, Kyushu University

HISANO, Masahiro
Department of Applied Science for Electronics and Materials, Kyushu University : Graduate Student

UTO, Keiko
Institute for Materials Chemistry and Engineering, and Research and Education Center of Green Technology, Kyushu University

HAYASHI, Jun-Ichiro
Institute for Materials Chemistry and Engineering, and Research and Education Center of Green Technology, Kyuhu University

他

https://doi.org/10.15017/5208234

出版情報：九州大学大学院総合理工学報告. 44 (2), pp.9-19, 2023-02. 九州大学大学院総合理工学府
バージョン：
権利関係：

九州大学大学院総合理工学府報告
第 44 巻 第 2 号 9-19 頁 令和 5 年 2 月

Engineering Sciences Reports, Kyushu University
Vol. 44, No. 2, pp. 9-19, FEB, 2023

Relative Formation Rate Constants and Electronic-State Distributions of Ne* Produced from the Ne^+/SF_6^- and $Ne^+/C_6F_6^-$ Ion-Ion Neutralization Reactions in the He Flowing Afterglow

Masaharu TSUJI*1,2† Masahiro HISANO*3 Keiko UTO*1
Jun-Ichiro HAYASHI*1 Takeshi TSUJI*4
†E-mail of corresponding author: tsuji@cm.kyushu-u.ac.jp

(Received October 31, 2022, accepted November 10, 2022)

Relative formation rate constants, $k_0(u)$, and electronic-state distributions, $N(u)$, of Ne* for upper u states in the Ne^+/SF_6^- and $Ne^+/C_6F_6^-$ ion-ion neutralization (I-IN) reactions were determined by observing Ne* atomic emissions in the 200–990 nm region. Ne* emissions from forty-two ns(n=4 and 5), ns'(n=4 and 5), np(n=3 and 4), np'(n=3 and 4), and 4d states in the 18.38–20.71 eV region were identified in the Ne^+/SF_6^- reaction, whereas those from forty-five ns(n=4 and 5), ns'(n=4 and 5), np(n=3 and 4), np'(n=3 and 4), nd(n=3–5), and nd'(n=3 and 4) states in the 18.38–21.02 eV region were observed in the $Ne^+/C_6F_6^-$ reaction. Major product Ne* states were 4s', 3d, and 3d' states in the Ne^+/SF_6^- reaction, whereas they were 3p, 4s', 3d, 3d', and 5d states in the $Ne^+/C_6F_6^-$ reaction. The electronic-state distributions of Ne* in the Ne^+/SF_6^- and $Ne^+/C_6F_6^-$ reactions suggested that Ne* atoms are not formed through long-lived Ne^+–SF_6^- and Ne^+–$C_6F_6^-$ complexes, where excess energies are distributed to products statistically. It was concluded that electronic-state distributions of Ne* are governed by the transition probability from the attractive Ne^+–SF_6^- and Ne^+–$C_6F_6^-$ entrance potentials to flat Ne*–SF_6 and Ne*–C_6F_6 exit potentials at crossing points.

Key words: *Neon ion, SF_6^-, $C_6F_6^-$, Ion-ion neutralization reaction, Flowing afterglow, Ne* atomic emission, Radiative cascade, Relative formation rate constant, Electronic-state distribution, Curve crossing*

1. Introduction

Due to a strong mutual Coulombic attractive force, reaction rate constants of recombination reactions between positive and negative ions are extremely large ($\alpha \approx 2 \times 10^{-7} \times (300/T)^{1/2}$ cm^3 s^{-1})[1,2] in comparison with those of ion–molecule reactions ($k \approx 10^{-11}$–10^{-9} cm^3 s^{-1}). Therefore, ion–ion reactions play a significant role as a loss process of ions in natural plasmas including interstellar gas clouds and in man-made plasmas such as static and flowing afterglows and laser plasmas. Until now reaction rate constants or cross sections of ion–ion reactions have been measured for various reaction systems, and several theoretical models have been proposed to explain the experimental data.[1-5] However, only very few optical spectroscopic studies have been carried out on the product-state distributions in ion–ion recombination reactions.[6,7]

Two-body ion–ion reactions between an atomic ion A and molecules BC leading to excited neutral species are classified into the following two cases:

Excimer formation via dissociative recombination reaction

$$A^+ + BC^- \rightarrow AB^* + C \quad (1)$$

Mutual neutralization reaction

$$A^+ + BC^- \rightarrow A^* + BC \quad (2)$$

*1 Institute for Materials Chemistry and Engineering, and Research and Education Center of Green Technology
*2 Department of Applied Science for Electronics and Materials
*3 Department of Applied Science for Electronics and Materials, Graduate Student
*4 Department of Materials Science, Shimane University

In process (1), a new A–B bond is created, while such a rearrangement does not occur, and only mutual neutralization takes place by an electron transfer from a negative ion to a positive ion in process (2).

We have previously studied the following two-body ion–ion recombination and neutralization reactions by using a flowing-afterglow method.[6-13)]

$$He^+ + C_6F_5X^- (X = F, Cl, Br, CF_3) \rightarrow He^* + C_6F_5F \quad (3)$$
$$Ar^+ + SF_6^- \rightarrow ArF^* + SF_5 \quad (4)$$
$$Kr^+ + SF_6^- \rightarrow KrF^* + SF_5 \quad (5a)$$
$$\rightarrow Kr^* + SF_6 \quad (5b)$$
$$Kr^+ + C_6F_6^- \rightarrow KrF^* + C_6F_5 \quad (6a)$$
$$\rightarrow Kr^* + C_6F_6 \quad (6b)$$
$$Xe^+ + SF_6^- \rightarrow XeF^* + SF_5 \quad (7)$$

In this study, the formation of Ne* in the Ne^+/SF_6^- and $Ne^+/C_6F_6^-$ I-IN reactions are investigated by observing Ne* emissions in the He flowing afterglow. The relative formation rate constants and electronic-state distributions are determined. The observed electronic-state distributions are compared with our previous results for the $He^+/C_6F_5X^-$ (X = F, Cl, Br, CF_3) I-IN reactions (3) leading to excited He* atoms.[13)] Based on the observed electronic-state distributions, reaction dynamics is discussed.

2. Experimental

The flowing-afterglow apparatus used in this study was essentially identical with that reported previously.[13,14)] We have previously studied Ne afterglow reactions of simple molecules.[15-18)] Then, we found that metastable $Ne(^3P_{0,2})$ atoms are major active species at low Ne buffer gas pressure below about 0.2 Torr (1 Torr = 133.3 Pa), whereas not only $Ne(^3P_{0,2})$ atoms but also Ne^+ and Ne_2^+ ions exist as active species at Ne gas pressures above that. The $[Ne_2^+]/[Ne^+]$ ratio increased with increasing the Ne gas pressure, because Ne_2^+ molecular ions are formed by the $Ne^+/2Ne$ three-body reaction.[20)]

$$Ne^+ + Ne + Ne \rightarrow Ne_2^+ + Ne \quad (8)$$
$$k_8 = (4.4\pm0.4) \times 10^{-32}\ cm^6\ s^{-1}$$

Both Ne^+ and Ne_2^+ can participate in the reaction as positive ion in the Ne afterglow at Ne gas pressures above 0.2 Torr. To exclude the contribution of Ne_2^+, we used here He afterglow reaction of Ne. We initially generated such He active species as $He(2^3S)$, He^+, and He_2^+ and electrons by a microwave discharge of high purity He gas (>99.9999%) in a He flowing afterglow at a microwave power of 100 W.[14,18)] The contribution of such charged species as He^+, He_2^+, and electrons to the observed emissions was examined by using a charged-particle collector grid placed between the discharge section and the reaction zone. A small amount of Ne gas (26 mTorr) was added from the first gas inlet placed 10 cm downstream from the center of microwave discharge. We used a low Ne partial pressure to suppress the formation of Ne_2^+ by the three-body reaction (9).

$$Ne^+ + Ne + He \rightarrow Ne_2^+ + He \quad (9)$$

The booster pump used in the present apparatus was equipped with a continuously variable gate valve. The flow tube pressure was varied from 0.9 Torr to 7.3 Torr by opening or closing the gate valve.

By the reactions of $He(2^3S)$, He^+, and He_2^+ with Ne, the following energy-transfer and charge-transfer reactions take place near the Ne gas inlet.[15,19,20)]

$$He(2^3S) + Ne \rightarrow Ne^*(4s,4s') + He \quad (10)$$
$$k_{10} = 3.85 \times 10^{-12}\ cm^3\ s^{-1}$$

$$He^+ + Ne \rightarrow Ne^+ + He \ (0.87) \quad (11a)$$
$$\rightarrow HeNe^+ + h\nu\ (0.17) \quad (11b)$$
$$k_{11a} = (1.20 \times 10^{-15}) \pm 30\%\ cm^3\ s^{-1}$$

$$He_2^+ + Ne \rightarrow Ne^+ + 2He \quad (12)$$
$$k_{12} = (6.00 \times 10^{-10}) \pm 30\%\ cm^3\ s^{-1}$$

Since the rate constant of reaction (12) is larger than that of (11) by five orders of magnitude, Ne^+ atomic ions are preferentially formed by reaction (12) in our He flowing-afterglow reaction of Ne.

We added an electron scavenger SF_6 or C_6F_6 from the second gas inlet placed further 10 cm downstream from the first gas inlet. The partial pressure of SF_6 or C_6F_6 was 3–5 mTorr. Around the second gas inlet, SF_6^- or $C_6F_6^-$ anions were formed by a fast electron attachment to SF_6 or C_6F_6,

$$e^- + SF_6 \rightarrow SF_6^- \quad (13)$$
$$k_{13} = 2.2 \times 10^{-7}\ cm^3\ s^{-1} \quad \text{(Ref. 21)}$$

$$e^- + C_6F_6 \rightarrow C_6F_6^- \quad (14)$$
$$k_{14} = 2.1 \times 10^{-7}\ cm^3\ s^{-1} \quad \text{(Ref. 22)}$$

Then, excited Ne* atoms can be formed through the following I-IN reactions around the second gas inlet:

$$Ne^+ + SF_6^- \rightarrow Ne^* + SF_6 \quad (15)$$
$$Ne^+ + C_6F_6^- \rightarrow Ne^* + C_6F_6 \quad (16)$$

Under our experimental conditions, excited Ne* states can be formed by energy-transfer reaction (10) and I-IN reaction (15) or (16). Without applying an electrostatic potential to the charged-particle collector grids, Ne* emissions resulting from both reactions (10) and (15) or (16) are observed, whereas those resulting only from reaction (10) are obtained by applying an electrostatic static potential to grids. Thus, the Ne* emissions resulting only from I-IN reaction (15) or (16) are obtained by subtracting the contribution of energy-transfer reaction (10). There are two spin-orbit components in the ground state of Ne^+, $^2P_{3/2}$ and $^2P_{1/2}$, with recombination energies of 21.56 and 21.66 eV, respectively. Their relative concentration was not estimated in this study.

A reaction flame around the second gas inlet was dispersed in the 200–990 nm region with a Spex 1250M monochromator equipped with cooled photomultipliers (Hamamatsu Photonics R376 and R316-02). The monochromator and the optical detection system were corrected by using standard D_2 and halogen lamps. All spectra presented here were corrected for the wavelength response of the detection system.

3. Results and Discussion

3.1 Emission spectra of Ne* resulting from the Ne^+/SF_6^- and $Ne^+/C_6F_6^-$ I-IN reactions

Figure 1(a) shows a typical emission spectrum resulting from the He(2^3S)/Ne + Ne^+/SF_6^- reactions in the 500–700 nm region at a He gas pressure of 7.3 Torr, where Ne* lines from the 3*p*, 3*p*′, 4*d*, and 5*s*′ states and a He line are identified. Most of the observed Ne* lines become weak, when charged species were removed from the He afterglow on applying an electrostatic potential to the grid, as shown in Fig. 1(b). Emission spectrum resulting from the Ne^+/SF_6^- I-IN reaction is shown in Fig. 1(c), which is obtained by subtracting spectrum (b) from spectrum (a).

The upper electronic states of the observed Ne* lines in the 500–970 nm region and their excitation energies are listed in Table 1. The spectral assignment was made by referring to reported atomic spectral tables,[23,24] and the excitation energies of Ne* were obtained from reported tables.[24,25] In the present study, we identified forty-two *ns*(*n*=4 and 5), *ns*′ (*n*=4 and 5), *np*(*n*=3 and 4), *np*′ (*n*=3 and 4), and 4*d* levels of Ne* in the 18.38–20.71 eV region. The recombination energies of $Ne^+(^2P_{3/2})$ and $Ne^+(^2P_{1/2})$ are 21.56 and 21.66 eV, respectively, and the electron affinity of SF_6 is 1.03 eV.[26] Therefore, the total available energies in the $Ne^+(^2P_{3/2})/SF_6^-$ and $Ne^+(^2P_{1/2})/SF_6^-$ I-IN reactions, $\Delta H_0^o + 3RT$, are 20.62 eV and 20.71 eV, respectively.

$$Ne^+(^2P_{3/2}) + SF_6^- \rightarrow Ne(^1S_0) + SF_6 + 20.54\ eV \quad (17a)$$
$$Ne^+(^2P_{1/2}) + SF_6^- \rightarrow Ne(^1S_0) + SF_6 + 20.63\ eV \quad (17b)$$

Low-energy Ne* states in the 18.38–20.57 eV region can be produced through both the $Ne^+(^2P_{3/2})/SF_6^-$ and $Ne^+(^2P_{1/2})/SF_6^-$ reactions. On the other hand, high energy Ne* states in the 20.66–20.71 eV region can only be formed though the $Ne^+(^2P_{1/2})/SF_6^-$ reaction. These results show that the upper $Ne^+(^2P_{1/2})$ spin-orbit component participates in the formation of Ne* in our experimental condition. In Table 1, both *nL* and *nL*′ states of Ne* with $2p^5(^2P_{3/2})nL$

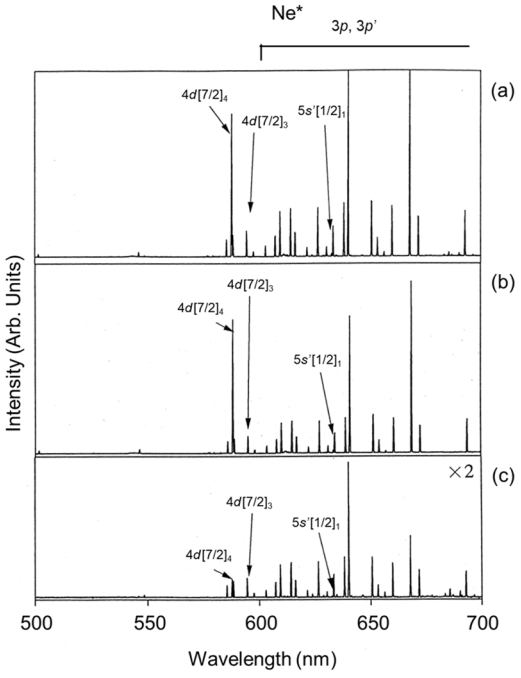

Fig. 1. Emission spectra resulting from (a) He(2^3S)/Ne + Ne^+/SF_6^-, (b) He(2^3S)/Ne, and (c) Ne^+/SF_6^- reactions in the 500–700 nm region.

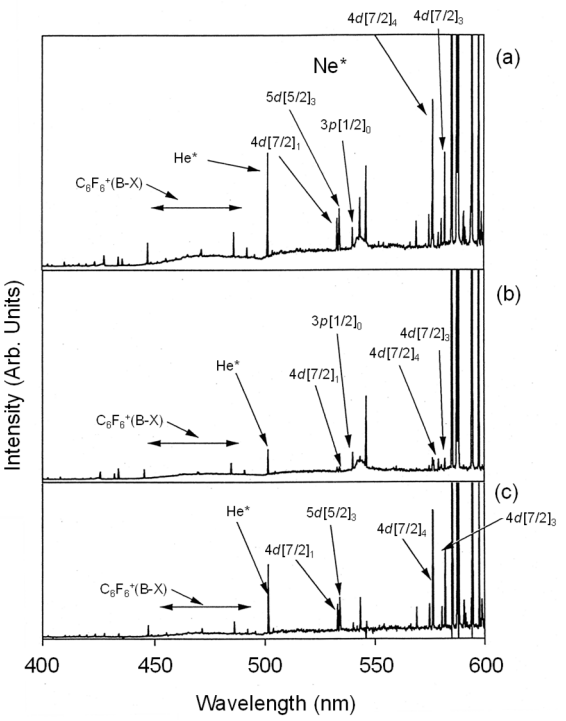

Fig. 2. Emission spectra resulting from (a) $He(2^3S)/Ne + Ne^+/C_6F_6^-$, (b) $He(2^3S)/Ne$, and (c) $Ne^+/C_6F_6^-$ reactions in the 400–600 nm region.

and $2p^5(^2P_{1/2})nL'$ (n=3–5, L=s, p, d) electron configurations, respectively, are produced. Based on this fact, Ne* states having both $Ne^+(^2P_{3/2})$ and $Ne^+(^2P_{1/2})$ ion-core configurations are formed in the Ne^+/SF_6^- reaction.

Figures 2(a)-2(c) show emission spectra resulting from the (a) $He(2^3S)/Ne + Ne^+/C_6F_6^-$, (b) $He(2^3S)/Ne$, and (c) $Ne^+/C_6F_6^-$ reactions in the 400–600 nm region at a He pressure of 0.91 Torr. Ne* lines from the 3p, 4d, and 5d states, a He* line, and $C_6F_6^+$(B-X) molecular ion emission[13,27] are observed. In Table 2 are listed the upper electronic states of the observed Ne* transitions in the 300–990 nm region and their excitation energies. In the present study, forty-five ns(n=4 and 5), ns' (n=4 and 5), np(n=3 and 4), np' (n=3 and 4), nd(n=3–5), and nd' (n=3 and 4) states of Ne* are identified with excitation energies of 18.38–21.02 eV. Since the electron affinity of C_6F_6 is 0.53 eV,[26] the total available energies in the $Ne^+(^2P_{3/2})/C_6F_6^-$ and $Ne^+(^2P_{1/2})/C_6F_6^-$ I-IN reactions, $\Delta H_0^o + 3RT$, are 21.11 eV and 21.21 eV, respectively.

$$Ne^+(^2P_{3/2}) + C_6F_6^- \rightarrow Ne(^1S_0) + C_6F_6 + 21.03\ eV \quad (18a)$$

$$Ne^+(^2P_{1/2}) + C_6F_6^- \rightarrow Ne(^1S_0) + C_6F_6 + 21.13\ eV \quad (18b)$$

Thus, all of the observed Ne* states in the 18.38–21.02 eV region can be produced through both the $Ne^+(^2P_{3/2})/C_6F_6^-$ and $Ne^+(^2P_{1/2})/C_6F_6^-$ reactions. The formation of both nL and nL' states of Ne* indicates that Ne* states having both $Ne^+(^2P_{3/2})$ and $Ne^+(^2P_{1/2})$ ion-core configurations are produced in the $Ne^+/C_6F_6^-$ reaction.

3.2 Relative formation rate constants and electronic-state distributions of Ne* in the Ne^+/SF_6^- and $Ne^+/C_6F_6^-$ I-IN reactions

The formation rate constant of an upper Ne* state, $k(u)$, and its steady-state electronic distribution, $N(u)$, in the Ne^+/SF_6^- and $Ne^+/C_6F_6^-$ reactions were evaluated from the emission intensity of a (u,l) transition of Ne*, I_{ul}, using similar relations given in the preceding paper for the $Ne^+/2e^-$ CRR reaction.[14]

$$[\mathrm{Ne}*(u)]/dt = k(u)[\mathrm{Ne}^+][\mathrm{X}^-] = k_0(u)[\mathrm{Ne}^+][\mathrm{X}^-] + \sum_h b_{hu}\, k(h)[\mathrm{Ne}^+][\mathrm{X}^-] \quad (19)$$

where X = SF_6 or C_6F_6, and b_{hu} is the optical branching ratio for the $h \rightarrow u$ radiative cascade transition:

Equation (19) gives

$$k(u) = k_0(u) + \sum_h b_{hu}\, k(h) = k_0(u) + k(u\text{: cascade}). \quad (20)$$

The rate constant for the direct excitation of a u level, $k_0(u)$, is deduced from Eq. (20), and the corresponding population, $N(u)$, is calculated from the relation:

$$N(u) \propto k_0(u) / \sum_l A_{ul} \quad (21)$$

In Tables 1 and 2 are given $k(u)$, $k(u\text{: cascade})$, $k_0(u)$, and $N(u)$ values for the Ne^+/SF_6^- and $Ne^+/C_6F_6^-$ reactions obtained from total intensities of observed emission lines and unobserved lines, respectively. Intensities of unobserved lines were estimated from intensities of observed lines and reported A_{ul} values for the same upper levels.[24] Figures 3 and 4 show the dependence of $k(u)$,

Table 1. Relative formation rate constants and electronic-state distribution of Ne* in the Ne^+/SF_6^- I-IN reaction in the He flowing afterglow.

Energy / eV	State	J	$k(u)$	$k(u:\text{cascade})$	$k_0(u)$	$N(u)$	$\ln(N(u)/g_u)$	$\sum_l A_{ul}$ $(s^{-1})^{a)}$
18.38	$3p$[1/2]	1	1.11E-01	8.87E-02	2.26E-02	3.94E-02	-4.33	3.93E+07
18.56	$3p$[5/2]	3	1.00E-01	1.00E-01	0.00E+00			5.15E+07
18.58	$3p$[5/2]	2	7.15E-02	7.15E-02	0.00E+00			4.90E+07
18.61	$3p$[3/2]	1	2.34E-01	2.34E-01	0.00E+00			5.12E+07
18.64	$3p$[3/2]	2	8.79E-02	8.79E-02	0.00E+00			4.98E+07
18.69	$3p'$[3/2]	1	5.13E-01	5.13E-01	0.00E+00			5.08E+07
18.70	$3p'$[3/2]	2	2.06E-01	2.06E-01	0.00E+00			5.27E+07
18.71	$3p$[1/2]	0	1.32E-02	1.32E-02	0.00E+00			6.06E+07
18.73	$3p'$[1/2]	1	2.46E-01	2.46E-01	0.00E+00			5.49E+07
18.97	$3p'$[1/2]	0	1.86E-02	1.86E-02	0.00E+00			6.24E+07
19.66	$4s$[3/2]°	2	1.04E-01	3.73E-02	6.66E-02	1.81E-01	-3.32	2.52E+07
19.76	$4s'$[1/2]°	0	2.93E-02		2.93E-02	7.98E-02	-2.53	2.52E+07
19.78	$4s'$[1/2]°	1	1.00E+00		1.00E+00	5.77E-01	-1.65	1.19E+08
20.03	$3d$[1/2]°	1	2.45E-02		2.45E-02	2.18E-02	-4.93	7.71E+07
20.03	$3d$[7/2]°	4	3.95E-02		3.95E-02	5.43E-02	-5.11	4.99E+07
20.03	$3d$[7/2]°	3	2.45E-02		2.45E-02	3.46E-02	-5.31	4.85E+07
20.04	$3d$[3/2]°	2	1.06E-02		1.06E-02	1.44E-02	-5.85	5.05E+07
20.04	$3d$[3/2]°	1	9.80E-02		9.80E-02	5.53E-02	-3.99	1.22E+08
20.05	$3d$[5/2]°	2	6.78E-02		6.78E-02	9.98E-02	-3.91	4.66E+07
20.05	$3d$[5/2]°	3	1.95E-02		1.95E-02	2.87E-02	-5.50	4.66E+07
20.14	$3d'$[5/2]°	2	7.09E-01		7.09E-01	1.00E+00	-1.61	4.86E+07
20.14	$3d'$[5/2]°	3	1.00E-02		1.00E-02	1.43E-02	-6.19	4.79E+07
20.14	$3d'$[3/2]°	2	2.89E-01		2.89E-01	4.08E-01	-2.51	4.85E+07
20.15	$4p$[1/2]	1	1.05E-03	1.05E-03	0.00E+00			4.84E+06
20.19	$4p$[5/2]	3	1.07E-03	1.07E-03	0.00E+00			7.35E+06
20.20	$4p$[5/2]	2	3.94E-03	3.94E-03	0.00E+00			7.01E+06
20.21	$4p$[3/2]	1	2.40E-03	2.40E-03	0.00E+00			7.77E+06
20.21	$4p$[3/2]	2	1.99E-03	1.99E-03	0.00E+00			8.81E+06
20.26	$4p$[1/2]	0	7.31E-04	7.31E-04	0.00E+00			1.14E+07
20.29	$4p'$[3/2]	1	1.41E-03	1.41E-03	0.00E+00			7.67E+06
20.30	$4p'$[1/2]	1	9.19E-04	9.19E-04	0.00E+00			8.40E+06
20.30	$4p'$[3/2]	2	2.46E-03	2.46E-03	0.00E+00			7.55E+06
20.37	$4p'$[1/2]	0	3.09E-04	3.09E-04	0.00E+00			1.58E+07
20.56	$5s$[3/2]°	2	1.54E-03		1.54E-03	8.01E-03	-6.44	1.32E+07
20.57	$5s$[3/2]°	1	8.09E-02		8.09E-02	1.07E-01	-3.34	5.20E+07
20.66	5s'[1/2]°	1	3.45E-02		3.45E-02	5.77E-02	-3.95	4.10E+07
20.70	$4d$[1/2]°	1	1.72E-03		1.72E-03	1.78E-03	-7.43	6.60E+07
20.71	$4d$[7/2]°	4	1.67E-03		1.67E-03	6.35E-03	-7.26	1.81E+07
20.71	$4d$[7/2]°	3	1.47E-03		1.47E-03	5.84E-03	-7.09	1.73E+07
20.71	$4d$[3/2]°	2	1.40E-03		1.40E-03	5.29E-03	-6.85	1.82E+07
20.71	$4d$[5/2]°	2	4.73E-04		4.73E-04	1.91E-03	-7.87	1.69E+07
20.71	$4d$[5/2]°	3	7.38E-04		7.38E-04	2.98E-03	-7.76	1.70E+07

[a)] Ref. 24. $\sum_l A_{ul}$ is the Einstein coefficient for spontaneous emission.

Table 2. Relative formation rate constants and electronic-state distribution of Ne* in the $Ne^+/C_6F_6^-$ I-IN reaction in the He flowing afterglow.

Energy / eV	State	J	$k(u)$	$k(u:\text{cascade})$	$k_0(u)$	$N(u)$	$\ln(N(u)/g_u)$	ΣA_i (s^{-1}) [a]
18.38	$3p$[1/2]	1	1.82E-01	7.58E-02	1.06E-01	3.22E-01	-2.23	3.93E+07
18.56	$3p$[5/2]	3	1.63E-01	1.12E-01	5.14E-02	1.19E-01	-4.08	5.15E+07
18.58	$3p$[5/2]	2	1.14E-01	7.13E-02	4.26E-02	1.03E-01	-3.88	4.90E+07
18.61	$3p$[3/2]	1	1.11E-01	1.11E-01	0.00E+00			5.12E+07
18.64	$3p$[3/2]	2	8.62E-02	8.35E-02	2.76E-03	6.59E-03	-6.63	4.98E+07
18.69	$3p'$[3/2]	1	1.87E-01	1.87E-01	0.00E+00			5.08E+07
18.70	$3p'$[3/2]	2	1.43E-01	1.43E-01	0.00E+00			5.27E+07
18.71	$3p$[1/2]	0	2.18E-02	2.18E-02	0.00E+00			6.06E+07
18.73	$3p'$[1/2]	1	1.48E-01	1.48E-01	0.00E+00			5.49E+07
18.97	$3p'$[1/2]	0	2.49E-02	2.49E-02	0.00E+00			6.24E+07
19.66	$4s$[3/2]°	2	1.31E-01	5.00E-02	8.07E-02	3.81E-01	-2.58	2.52E+07
19.69	$4s$[3/2]°	1	5.54E-02	2.28E-04	5.52E-02	6.78E-02	-3.79	9.68E+07
19.76	$4s'$[1/2]°	0	7.18E-02	2.88E-04	7.15E-02	3.38E-01	-1.09	2.52E+07
19.78	$4s'$[1/2]°	1	1.00E+00	8.53E-04	9.99E-01	1.00E+00	-1.10	1.19E+08
20.03	$3d$[1/2]°	1	2.83E-02	3.91E-06	2.83E-02	4.36E-02	-4.23	7.71E+07
20.03	$3d$[7/2]°	4	3.38E-02		3.38E-02	8.06E-02	-4.72	4.99E+07
20.03	$3d$[7/2]°	3	2.07E-02	4.65E-07	2.07E-02	5.07E-02	-4.93	4.85E+07
20.04	$3d$[3/2]°	2	1.17E-02	7.54E-07	1.17E-02	2.75E-02	-5.20	5.05E+07
20.04	$3d$[3/2]°	1	1.49E-01		1.49E-01	1.45E-01	-3.03	1.22E+08
20.05	$3d$[5/2]°	2	1.30E-02		1.30E-02	3.31E-02	-5.02	4.66E+07
20.05	$3d$[5/2]°	3	2.33E-02		2.33E-02	5.94E-02	-4.77	4.66E+07
20.14	$3d'$[5/2]°	2	1.64E-01		1.64E-01	4.01E-01	-2.52	4.86E+07
20.14	$3d'$[3/2]°	2	1.14E-01		1.14E-01	2.80E-01	-2.88	4.85E+07
20.14	$3d'$[3/2]°	1	2.34E-02		2.34E-02	3.29E-02	-4.51	8.47E+07
20.15	$4p$[1/2]	1	1.88E-03	1.88E-03	0.00E+00			4.84E+06
20.19	$4p$[5/2]	3	4.21E-03	4.21E-03	0.00E+00			7.35E+06
20.20	$4p$[5/2]	2	1.33E-02	1.33E-02	0.00E+00			7.01E+06
20.21	$4p$[3/2]	1	1.76E-02	1.76E-02	0.00E+00			7.77E+06
20.21	$4p$[3/2]	2	2.13E-03	2.13E-03	0.00E+00			8.81E+06
20.26	$4p$[1/2]	0	7.06E-04	7.06E-04	0.00E+00			1.14E+07
20.29	$4p'$[3/2]	1	5.51E-03	5.51E-03	0.00E+00			7.67E+06
20.30	$4p'$[1/2]	1	4.69E-03	4.69E-03	0.00E+00			8.40E+06
20.30	$4p'$[3/2]	2	1.25E-02	1.25E-02	0.00E+00			7.55E+06
20.37	$4p'$[1/2]	0	1.67E-03	1.67E-03	0.00E+00			1.58E+07
20.56	$5s$[3/2]°	2	6.83E-03		6.83E-03	6.16E-02	-4.40	1.32E+07
20.57	$5s$[3/2]°	1	1.97E-02		1.97E-02	4.51E-02	-4.20	5.20E+07
20.66	$5s'$[1/2]°	1	1.74E-01		1.74E-01	5.05E-01	-1.78	4.10E+07
20.70	$4d$[1/2]°	1	5.30E-03		5.30E-03	9.55E-03	-5.75	6.60E+07
20.71	$4d$[7/2]°	4	5.45E-03		5.45E-03	3.58E-02	-5.53	1.81E+07
20.71	$4d$[7/2]°	3	4.21E-03		4.21E-03	2.90E-02	-5.49	1.73E+07
20.71	$4d$[3/2]°	2	3.21E-03		3.21E-03	2.10E-02	-5.47	1.82E+07
20.71	$4d$[5/2]°	2	3.89E-02		3.89E-02	2.73E-01	-2.91	1.69E+07
20.81	$4d'$[3/2]°	1	2.12E-03		2.12E-03	5.79E-03	-6.25	4.35E+07
21.02	$5d$[7/2]°	3	3.54E-03		3.54E-03	6.49E-02	-4.68	6.48E+06
21.02	$5d$[5/2]°	2	3.39E-02		3.39E-02	6.34E-01	-2.07	6.36E+06

[a] Ref. 24. $\sum_l A_{ul}$ is the Einstein coefficient for spontaneous emission.

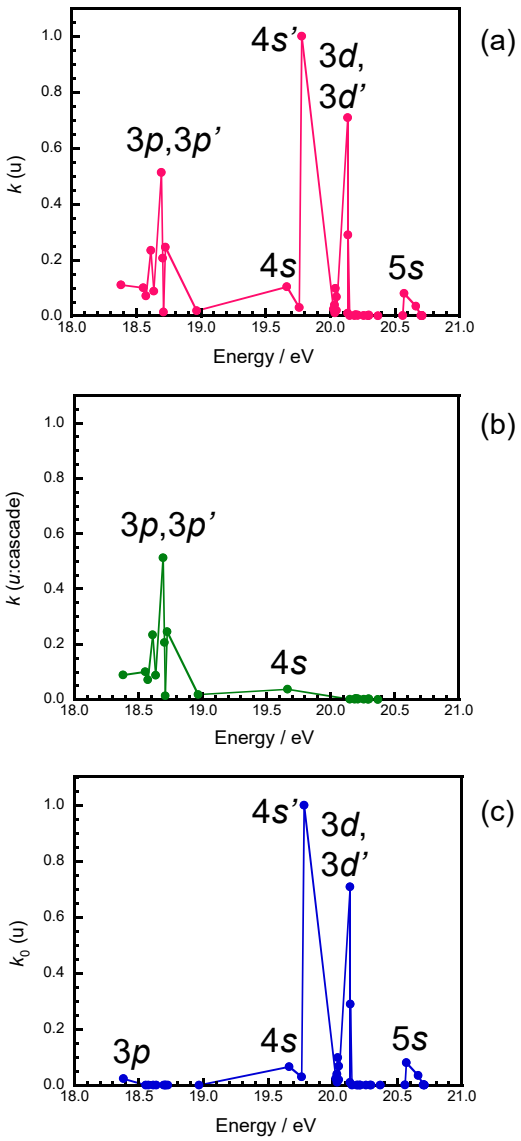

Fig. 3. Dependence of relative formation rate constants on the excitation energy of Ne* in the Ne^+/SF_6^- reaction: (a) including radiative cascade, (b) radiative cascade, and (c) excluding radiative cascade.

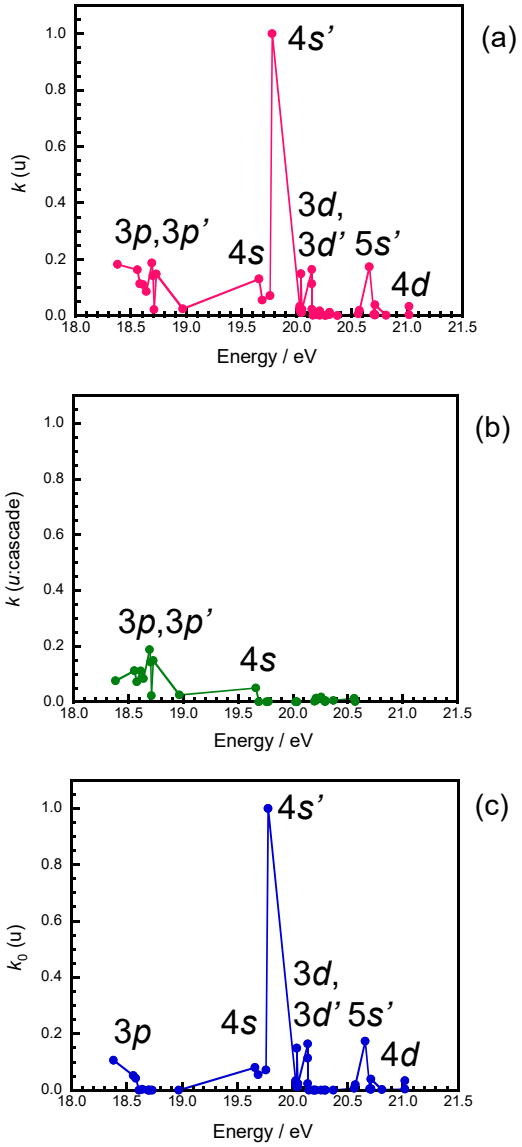

Fig. 4. Dependence of relative formation rate constants on the excitation energy of Ne* in the $Ne^+/C_6F_6^-$ reaction: (a) including radiative cascade, (b) radiative cascade, and (c) excluding radiative cascade.

$k(u:cascade)$, and $k_0(u)$ values on the excitation energy of Ne* in the Ne^+/SF_6^- and $Ne^+/C_6F_6^-$ reactions, respectively. A comparison between $k(u)$ and $k_0(u)$ values in Tables 1 and 2, and Figs. 3 and 4 suggests that some $3p$ and all $3p'$, $4p$, and $4p'$ levels are formed only through radiative cascade from upper levels in the Ne^+/SF_6^- and $Ne^+/C_6F_6^-$ reactions. The cascade-free $k_0(u)$ values indicate that favorable states in the Ne^+/SF_6^- reaction are $4s'$, $3d$, and $3d'$ states, whereas those in the $Ne^+/C_6F_6^-$ reaction are $3p$, $4s$, $4s'$, $3d$, $3d'$, and $5s'$ states. Among them, the $4s'$ state at 19.78 eV is the most favorable in both reactions.

Figures 5, 6 and 7, 8 show the dependence of $N(u)$ and $\ln(N(u)/g_u)$ on the excitation energy of Ne* in the Ne^+/SF_6^- and $Ne^+/C_6F_6^-$ reactions, respectively. Favorable populations are obtained for the $4s$, $4s'$, $3d$, $3d'$, and $5s$ in the Ne^+/SF_6^- reaction, whereas they are found for the $3p$, $4s$, $4s'$, $3d$, $3d'$, $5s'$, and $5d$ states in the $Ne^+/C_6F_6^-$ reaction. It should be noted that the most populated states are different between the two reactions. They are the $3d'$ state at 20.14 eV in the Ne^+/SF_6^- reaction and the $4s'$ state at 19.78 eV in the $Ne^+/C_6F_6^-$ reaction.

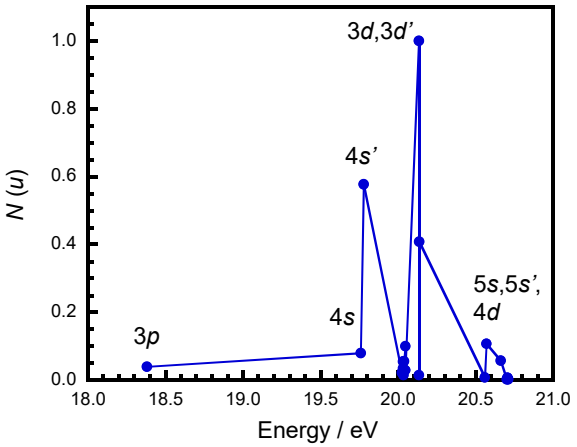

Fig. 5. Electronic-state distribution vs exciation energy of Ne* in the Ne^+/SF_6^- reaction.

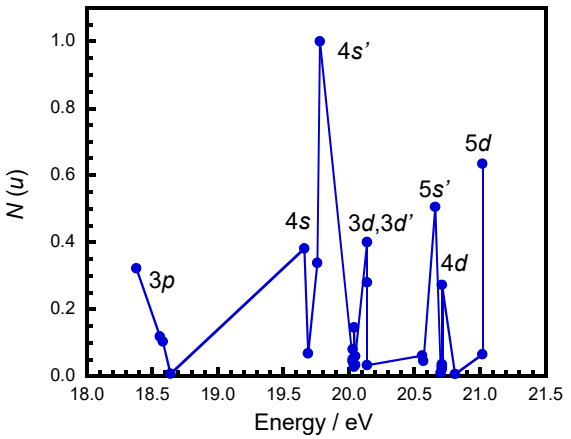

Fig. 7. Electronic-state distribution vs exciation energy of Ne* in the $Ne^+/C_6F_6^-$ reaction.

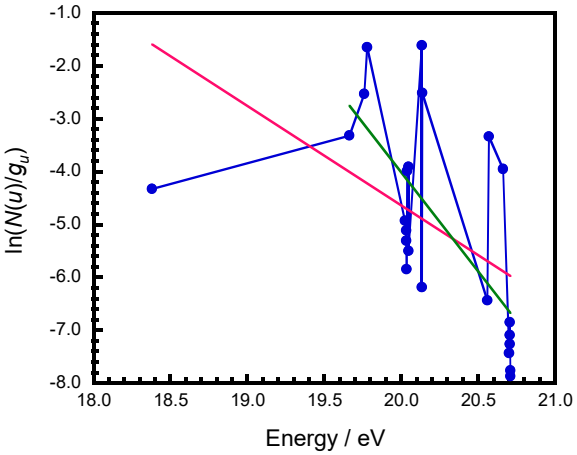

Fig. 6. $\ln(N(u)/g_u)$ vs excitation energy of Ne* in the Ne^+/SF_6^- reaction.

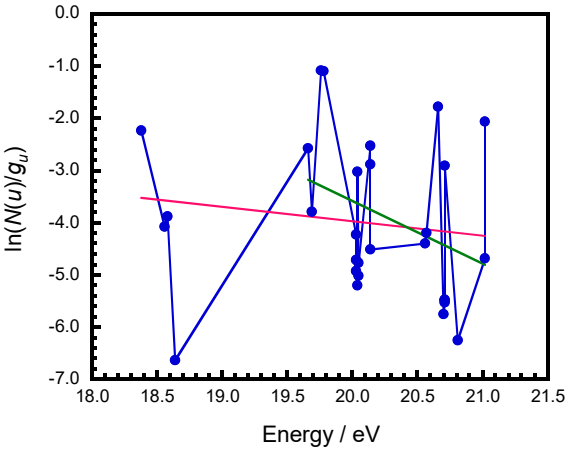

Fig. 8. $\ln(N(u)/g_u)$ vs exciation energy of Ne* in the $Ne^+/C_6F_6^-$ reaction.

In Tables 3 and 4 are summarized the total relative formation rate constants ($\sum_u k_0(u)$) and electronic-state distributions ($\sum_u N(u)$) of Ne* in the Ne^+/SF_6^- and $Ne^+/C_6F_6^-$ reactions at thermal energy. Based on the present data shown in these tables, major populated Ne* states in the Ne^+/SF_6^- reaction are the 4*s*′, 3*d*, and 3*d*′ states, which occupy 40.6, 11.2, and 39.8% of $\sum_u k_0(u)$ and 23.4, 11.0, and 50.7% of $\sum_u N(u)$, respectively. On the other hand, major populated Ne* states in the $Ne^+/C_6F_6^-$ reaction are the 3*p*, 4*s*′, 3*d*, 3*d*′, 5*s*′, and 5*d* states, which occupy 8.9, 46.8, 12.2, 13.2, 7.6, and 1.6% of $\sum_u k_0(u)$ and 10.6, 25.9, 8.5, 13.8, 9.8, and 13.5% of $\sum_u N(u)$, respectively. These results suggest that Ne* states formed in the $Ne^+/C_6F_6^-$ reaction are populated in more wider energy range than those produced in the Ne^+/SF_6^- reaction. One reason for this is the larger total available energy of the $Ne^+/C_6F_6^-$ reaction than that of the Ne^+/SF_6^- reaction, so that higher energy Ne* states can be formed.

The $\sum_u k_0(u)$ and $\sum_u N(u)$ values of the product states having the $Ne^+(^2P_{3/2})$ ion core and the $Ne^+(^2P/_{1/2})$ ion core are 18:82% and 24:76%, for the Ne^+/SF_6^- reaction, whereas they are 32:68% and 50:50% for the $Ne^+/C_6F_6^-$ reaction, respectively. Since both $^2P_{3/2}$ and $^2P_{1/2}$ spin-orbit components of Ne^+ exist in the present experiment and their relative concentration is not determined. Therefore, it is difficult to discuss the relative contribution of the $Ne^+(^2P_{3/2})$ and $Ne^+(^2P_{1/2})$ components and conservation of ion-core configuration during the I-IN reactions. One of the spin-orbit components must be selected to discuss further the electron-transfer mechanism in these reaction systems.

Assuming a Maxwell–Boltzmann distribution, N_u is given by

Table 3. Total relative formation rate constants and electronic-state distribution of Ne* in the Ne^+/SF_6^- I-IN reaction at thermal energy.

State	Number of sublevel	$\sum_u k_0(u)$ (%)	$\sum_u N(u)$ (%)
3*p*	1	0.9	1.4
4*s*	1	2.6	6.5
4*s*′	2	40.6	23.4
3*d*	7	11.2	11.0
3*d*′	3	39.8	50.7
5*s*	2	3.3	4.1
5*s*′	1	1.4	2.1
4*d*	6	0.3	0.9

Table 4. Total relative formation rate constants and electronic-state distribution of Ne* in the $Ne^+/C_6F_6^-$ I-IN reaction at thermal energy.

State	Number of sublevel	$\sum_u k_0(u)$ (%)	$\sum_u N(u)$ (%)
3*p*	4	8.9	10.6
4*s*	2	5.9	8.7
4*s*′	2	46.8	25.9
3*d*	7	12.2	8.5
3*d*′	3	13.2	13.8
5*s*	2	1.2	2.1
5*s*′	1	7.6	9.8
4*d*	5	2.5	7.1
4*d*′	1	0.1	0.1
5*d*	2	1.6	13.5

$$N_u = g_u \exp(-E_u/kT_e), \qquad (22)$$

where E_u is the excitation energy of Ne*. If a plot of $\ln(N_u/g_u)$ vs E_u is linear, then the distribution can be characterized by a Boltzmann electronic temperature (T_e). The dependence of $\ln(N_u/g_u)$ on E_u was fitted by straight lines as shown in Figs. 5 and 6. Although deviations from linearity are large in the present systems, Boltzmann electronic temperatures of 0.53 and 0.27 eV were obtained from slopes of the straight lines for Ne* from the Ne^+/SF_6^- reaction in the whole 18.4–20.7 eV region and high-energy 19.7–20.7 eV region, respectively. On the other hand, Boltzmann temperatures of 3.63 and 0.83 eV were obtained for Ne* from the $Ne^+/C_6F_6^-$ reaction in the whole 18.4–21.0 eV region and high-energy 19.7–21.0 eV region, respectively. We have previously obtained Boltzmann electronic temperatures of 0.070, 0.16, 0.090, and 0.19 eV for He* from the $He^+/C_6F_5X^-$ (X=F, Cl, Br, and CF_3) I-IN reactions, respectively.[13] Thus, the Boltzmann electronic temperatures obtained for Ne* from the Ne^+/SF_6^- and $Ne^+/C_6F_6^-$ reactions are higher than those of the $He^+/C_6F_5X^-$ reactions.

It should be noted that many points are far from the line of best fit in Figs. 6 and 8. Thus, very small R^2 (coefficient of determination) values of 0.26 and 0.018 are obtained for the Ne^+/SF_6^- reaction in the 18.4–20.7 eV region and for the $Ne^+/C_6F_6^-$ reaction 19.7–20.7 eV region, respectively. It is therefore reasonable to assume that reaction dynamics of Ne^+/SF_6^- and $Ne^+/C_6F_6^-$ I-IN reactions is not governed by statistical model, where such long-lived intermediates as Ne^+–SF_6^- and Ne^+–$C_6F_6^-$ are formed and excess energies are distributed to all degrees of freedom statistically. Curve crossings between strongly attractive entrance Ne^+–SF_6^- and Ne^+–$C_6F_6^-$ curves and rather flat Ne*–SF_6 and Ne*–C_6F_6 exit curves and the probability of an electron transfer from an anion to a cation at crossing points would play a significant role for the electronic-state distributions of the present two I-IN reactions.

The crossing points R_c (Å) were calculated from the relation

$$R_c = e^2/(\mathrm{IP}-\mathrm{EA}) = 14.38/(\mathrm{IP}-\mathrm{EA}), \qquad (23)$$

where IP is the ionization potential of Ne* and EA is the electron affinity of X. The R_c values calculated for the formation of each Ne* state in the Ne^+/SF_6^- and $Ne^+/C_6F_6^-$ reactions are given in Tables 5 and 6. Most of the product states are produced via curve crossings at interparticle distances of 15–37 Å in the Ne^+/SF_6^- reaction, whereas they are curve crossings at 5–38 Å in the $Ne^+/C_6F_6^-$ reaction. According to Landau–Zener theory, the probability of electron transfer falls off rapidly at large R_c because of the rapidly diminishing nonadiabatic coupling matrix elements, and therefore the reaction efficiencies of such high energy states as 5*s*, 5*s*′, 4*d*, and 4*d*′ would be small.

Based on the *ab initio* calculation of SF_6^-, the singly occupied molecular orbital (SOMO) of SF_6^- is totally symmetric a_{1g} with S(3s)–F(2pσ*) character.[28] On the other hand, ESR data in the condensed phase demonstrated that the SOMO of $C_6F_6^-$ has σ* character.[29] Since

Table 5. Curve crossing points between entrance $Ne^+(^2P_{3/2,1/2})$–SF_6^- and exit Ne*–SF_6 potentials.

Energy / eV	State	R_c (Å) $Ne^+(^2P_{3/2})$ /SF_6^-	R_c (Å) $Ne^+(^2P_{1/2})$ /SF_6^-
18.38	3*p*[1/2]	6.69	6.40
19.66	4*s*[3/2]°	16.61	14.89
19.76	4*s*′[1/2]°	18.69	16.54
19.78	4*s*′[1/2]°	19.17	16.91
20.03	3*d*[1/2]°	28.56	23.82
20.03	3*d*[7/2]°	29.03	24.15
20.03	3*d*[7/2]°	29.04	24.16
20.04	3*d*[3/2]°	29.15	24.24
20.04	3*d*[3/2]°	29.37	24.39
20.05	3*d*[5/2]°	29.84	24.72
20.05	3*d*[5/2]°	29.86	24.72
20.14	3*d*′[5/2]°	36.50	29.11
20.14	3*d*′[5/2]°	36.52	29.12
20.14	3*d*′[3/2]°	36.63	29.20
20.56	5*s*[3/2]°		205.55
20.57	5*s*[3/2]°		241.81

I-IN reactions occur via an electron transfer from an anion to a cation, the overlapping between the SOMO orbital with S–F or C–F σ* character and a vacant orbital to which an electron is transferred at the crossing point will be significant for the final state distribution of Ne*.

4. Summary and Conclusion

The Ne^+/SF_6^- and $Ne^+/C_6F_6^-$ ion-ion mutual neutralization reactions were studied by observing Ne* lines in the He afterglow. Ne* emissions from forty-two *ns*(*n*=4 and 5), *ns*′(*n*=4 and 5), *np*(*n*=3 and 4), *np*′(*n*=3 and 4), and 4*d* states of Ne* in the 18.38–20.71 eV region were identified in the Ne^+/SF_6^- reaction, whereas those from forty-five *ns*(*n*=4 and 5), *ns*′(*n*=4 and 5), *np*(*n*=3 and 4), *np*′(*n*=3 and 4), *nd*(*n*=3–5), and *nd*′(*n*=3 and 4) states of Ne* in the 18.38–21.02 eV region are observed in the $Ne^+/C_6F_6^-$ reaction. Major product Ne* states in the Ne^+/SF_6^- reaction are 4*s*′, 3*d,* and 3*d*′ states, whereas those in the $Ne^+/C_6F_6^-$ reaction are 3*p*, 4*s*′, 3*d,* 3*d*′, and 5*d* states. The electronic-state distributions of Ne* in the Ne^+/SF_6^- and $Ne^+/C_6F_6^-$ reactions were not expressed by a single Boltzmann distribution. Therefore, it was concluded that the reaction dynamics is mainly controlled by transition probability between the strongly attractive Ne^+–X^- ion-pair potentials and rather flat exit Ne*–X potentials at relatively large crossing points.

Table 6. Curve crossing points between entrance $Ne^+(^2P_{3/2,1/2})$–$C_6F_6^-$ and exit Ne*–C_6F_6 potentials.

Energy / eV	State	R_c (Å) $Ne^+(^2P_{3/2})$ /$C_6F_6^-$	R_c (Å) $Ne^+(^2P_{1/2})$ /$C_6F_6^-$
18.38	3*p*[1/2]	5.41	5.21
18.56	3*p*[5/2]	5.79	5.56
18.58	3*p*[5/2]	5.84	5.61
18.64	3*p*[3/2]	5.98	5.74
19.66	4*s*[3/2]°	10.45	9.74
19.69	4*s*[3/2]°	10.64	9.90
19.76	4*s*′[1/2]°	11.24	10.42
19.78	4*s*′[1/2]°	11.41	10.57
20.03	3*d*[1/2]°	14.19	12.91
20.03	3*d*[7/2]°	14.30	13.01
20.03	3*d*[7/2]°	14.31	13.01
20.04	3*d*[3/2]°	14.33	13.03
20.04	3*d*[3/2]°	14.39	13.08
20.05	3*d*[5/2]°	14.50	13.17
20.05	3*d*[5/2]°	14.50	13.17
20.14	3*d*′[5/2]°	15.91	14.32
20.14	3*d*′[3/2]°	15.93	14.34
20.14	3*d*′[3/2]°	15.97	14.37
20.56	5*s*[3/2]°	29.96	24.79
20.57	5*s*[3/2]°	30.63	25.25
20.66	5*s*′[1/2]°	38.12	30.13
20.70	4*d*[1/2]°	42.58	32.85
20.71	4*d*[7/2]°	42.97	33.08
20.71	4*d*[7/2]°	42.99	33.09
20.71	4*d*[3/2]°	43.15	33.19
20.71	4*d*[5/2]°	43.74	33.54
20.81	4*d*′[3/2]°	61.32	42.99
21.02	5*d*[7/2]°	588.66	115.57
21.02	5*d*[5/2]°	670.25	118.40

We studied here Ne* formation from the Ne^+/SF_6^- and $Ne^+/C_6F_6^-$ I-IN reactions (15) and (16). In our previous studies on the Rg^+/SF_6^- (Rg=Ar, Kr, Xe) and $Rg^+/C_6F_6^-$ (Rg=Kr) reactions (4)–(7), RgF* (Rg=Ar, Kr, Xe) excimer emissions were observed as major products in most cases.[6-9,11] It has been known that NeF* excimer emission occurs in the vacuum ultraviolet (VUV) region (105–115 nm with a peak at 108 nm).[30] In the cases of Ne^+/SF_6^- and $Ne^+/C_6F_6^-$ reactions, the formation of NeF* excimer with a transition energy of 11.5 eV is energetically possible.

$$Ne^+ + SF_6^- \rightarrow NeF^* + SF_5 \quad (24)$$
$$Ne^+ + C_6F_6^- \rightarrow NeF^* + C_6F_5 \quad (25)$$

A further optical spectroscopic study in the VUV region is necessary to clarify whether excimer formation processes (24) and (25) compete with the formation of Ne* through I-IN processes (15) and (16) and their branching ratios. .

Acknowledgments

The authors acknowledge financial support from the Mitsubishi foundation (1996) and Kyushu University Interdisciplinary Programs in Education and Projects in Research Development (2001–2002). They also give thanks to Prof. Kenji Furuya for his careful reading of our manuscript.

References

1) D. R. Bates, *Adv. Atomic. Mol. Phys.*, 20, 1 (1985).
2) M. R. Flanney, *Adv. Atomic, Mol. Opt. Phys.*, 32, 117 (1994).
3) M. Zauner-Wieczorek, J. Curtius, and A. Kürten, *Atmos. Chem. Phys.*, 2021, https://doi.org/10.5194/acp-2021-795.
4) N. S. Shuman, T. M. Miller, R. Johnsen, and A. A. Viggiano, *J. Chem. Phys.*, 140, 044304 (2014).
5) J. P. Wiens, N. S. Shuman, T. M. Miller, and A. A. Viggiano, *J. Chem. Phys.*, 144, 204309 (2016).
6) M. Tsuji, *Trends Phys. Chem.*, 5, 25 (1995).
7) M. Tsuji, *Houshasenkagaku*, 62, 18 (1996).
8) M. Tsuji, M. Furusawa, and Y. Nishimura, *Chem. Phys. Lett.*, 166, 363 (1990).
9) M. Tsuji, M. Furusawa, and Y. Nishimura, *J. Chem. Phys.*, 92, 6502 (1990).
10) M. Tsuji, T, Muraoka, M. Ide, H. Ujita, Y. Nishimura, *J. Chem. Phys.*, 101, 2880 (1994).
11) M. Tsuji, H. Ishimi, and Y. Nishimura, *Chem. Lett.*, 25, 515 (1996).
12) M. Tsuji, M. Nakamura, and Y. Nishimura, *Chem. Lett.*, 26, 259 (1997).
13) M. Tsuji, M. Nakamura, Y. Nishimura, E. Oda, H. Oota, and M. Hisano, *J. Chem. Phys.*, 110, 2903 (1999).
14) M. Tsuji, M. Hisano, K. Uto, J.-I. Hayashi, and T. Tsuji, *Eng. Sci. Rep. Kyushu Univ.*, 44, 1 (2023).
15) M. Tsuji, M. Hisano, T. Tanoue, and Y. Nishimura, *Jpn. J. Appl. Phys.*, 39, 4970 (2000).
16) H. Sekiya, M. Tsuji, and Y. Nishimura *Chem. Phys. Lett.*, 100, 494 (1983).
17) H. Obase, M. Tsuji, and Y. Nishimura, *Chem. Phys. Lett.*, 105, 214 (1984).
18) M. Tsuji, "*Techniques of Chemistry: Techniques for the Study of Ion Molecule Reactions; Chapter IX. Spectroscopic Probes*", Edited by J. M. Farrar and W. Saunders, Jr., John Wiley & Sons, Inc, Publishers, 489 (1988).
19) A. L. Schmeltekoph and F. C. Fehsenfeld, *J. Chem. Phys.*, 53, 3173 (1974).
20) V. G. Anicich, "*An Index of the Literature for Bimolecular Gas Phase Cation-Molecule Reaction Kinetics*", JPL Publication, 03-19 NASA (2003), and references therein.
21) F. C. Fehsenfeld, *J. Chem. Phys.*, 53, 2000 (1970).
22) H. Shimamori, Y. Tatsumi, and T. Sunagawa, *J. Chem. Phys.*, 99, 7787 (1993).
23) A. R. Striganov and N. S. Sventitskii "*Tables of Spectral Lines of Neutral and Ionized Atoms*", Plenum Press, New York (1979).
24) *Atomic Spectra Database*, *NIST Standard Reference Database*, 78, Ver. 5.9. Oct. (2021).
25) C. E. Moore, "*Atomic Energy Levels*," U.S. GPO, Washington D.C., *Natl. Bur. Stand.* (U.S.) Circ. 467 (1949).
26) *NIST Chemistry WebBook*, *NIST Standard Reference Database*, Number 69 (2022) https://doi.org/10.18434/T4D303.
27) M. Allan and J. P. Maier, *Chem. Phys. Lett*, 34, 442 (1975).
28) J. A. Tossell, *Chem. Phys.*, 154, 211 (1991).
29) J. P. Rogers, C. S. Anstöter, J. N. Bull, B. F. E. Curchod, and J. R. R. Verlet, *J. Phys. Chem. A*, 123, 1602 (2019).
30) N. W. Winter, C. F. Bender, and T. N. Rescigno, *J. Chem. Phys.*, 67, 3122 (1977).